ADVANCED HEALTHCARE MATERIALS
www.advhealthmat.de

# A Biocompatible Therapeutic Catheter-Deliverable Hydrogel for In Situ Tissue Engineering

*Amanda N. Steele, Lyndsay M. Stapleton, Justin M. Farry, Haley J. Lucian, Michael J. Paulsen, Anahita Eskandari, Camille E. Hironaka, Akshara D. Thakore, Hanjay Wang, Anthony C. Yu, Doreen Chan, Eric A. Appel,* and Yiping Joseph Woo**

**Hydrogels have emerged as a diverse class of biomaterials offering a broad range of biomedical applications. Specifically, injectable hydrogels are advantageous for minimally invasive delivery of various therapeutics and have great potential to treat a number of diseases. However, most current injectable hydrogels are limited by difficult and time-consuming fabrication techniques and are unable to be delivered through long, narrow catheters, preventing extensive clinical translation. Here, the development of an easily-scaled, catheter-injectable hydrogel utilizing a polymer–nanoparticle crosslinking mechanism is reported, which exhibits notable shear-thinning and self-healing behavior. Gelation of the hydrogel occurs immediately upon mixing the biochemically modified hyaluronic acid polymer with biodegradable nanoparticles and can be easily injected through a high-gauge syringe due to the dynamic nature of the strong, yet reversible crosslinks. Furthermore, the ability to deliver this novel hydrogel through a long, narrow, physiologically-relevant catheter affixed with a 28-G needle is highlighted, with hydrogel mechanics unchanged after delivery. Due to the composition of the gel, it is demonstrated that therapeutics can be differentially released with distinct elution profiles, allowing precise control over drug delivery. Finally, the cell-signaling and biocompatibility properties of this innovative hydrogel are demonstrated, revealing its wide range of therapeutic applications.**

## 1. Introduction

Hydrogels are valuable tools in tissue engineering and regenerative medicine due to their biocompatibility, tunable mechanics, and ability to deliver an array of cells and biomolecules.[1–7] Hydrogels are defined as water-swollen, insoluble networks of crosslinked polymers, exhibiting high-water content, biomimetic elasticity, and tissue-like diffusion properties.[8–10] Cell and cytokine therapeutics can be significantly enhanced via encapsulation within hydrogels, due to stabilization during delivery, protection from the immune system in vivo, and localization to the intended delivery region, ultimately extending the therapeutic window.[2,9,11]

Historically, hydrogels have often utilized covalent crosslinking mechanisms, which can be damaging to encapsulated biologics due to processing techniques involving non-physiologic pH, cytotoxic chemicals, photosensitizers, or free radicals.[12–14] Furthermore, chemical crosslinks are generally permanent, and thus irreversible, limiting minimally-invasive application.[15–17] As a result, self-assembly via noncovalent cross-linking mechanisms has emerged as a promising approach to minimally invasive hydrogel delivery. Such systems include Dock-and-Lock hydrogels, leucine-zipper hydrogels, two-component protein motif recognition hydrogels, and host–guest interaction hydrogels.[3,18–23] In each of these platforms, dynamic and reversible crosslinking behavior was observed, allowing for injectability. However, the extent of shear-thinning and self-healing behavior of current injectable hydrogels is lacking, and synthesis of these hydrogels is difficult, expensive, and poorly scalable, significantly limiting clinical translation.

As a result, translation of injectable hydrogels must meet the following criteria: scalable formation, significant shear-thinning behavior, rapid self-healing, and biocompatibility. Recently, polymer—nanoparticle (NP) hydrogels have emerged as a promising method to develop tunable shear-thinning, self-healing materials that do not necessitate complex chemical

A. N. Steele, L. M. Stapleton, Dr. Y. J. Woo
Department of Bioengineering
Stanford University
Stanford, CA 94305, USA
E-mail: joswoo@stanford.edu
A. N. Steele, L. M. Stapleton, J. M. Farry, H. J. Lucian, M. J. Paulsen, A. Eskandari, C. E. Hironaka, A. D. Thakore, H. Wang, Dr. Y. J. Woo
Department of Cardiothoracic Surgery
Stanford University
Stanford, CA 94305, USA
A. C. Yu, D. Chan, Dr. E. A. Appel
Department of Materials Science & Engineering
Stanford University
Stanford, CA 94305, USA
E-mail: eappel@stanford.edu
The ORCID identification number(s) for the author(s) of this article can be found under https://doi.org/10.1002/adhm.201801147.

**DOI: 10.1002/adhm.201801147**

 

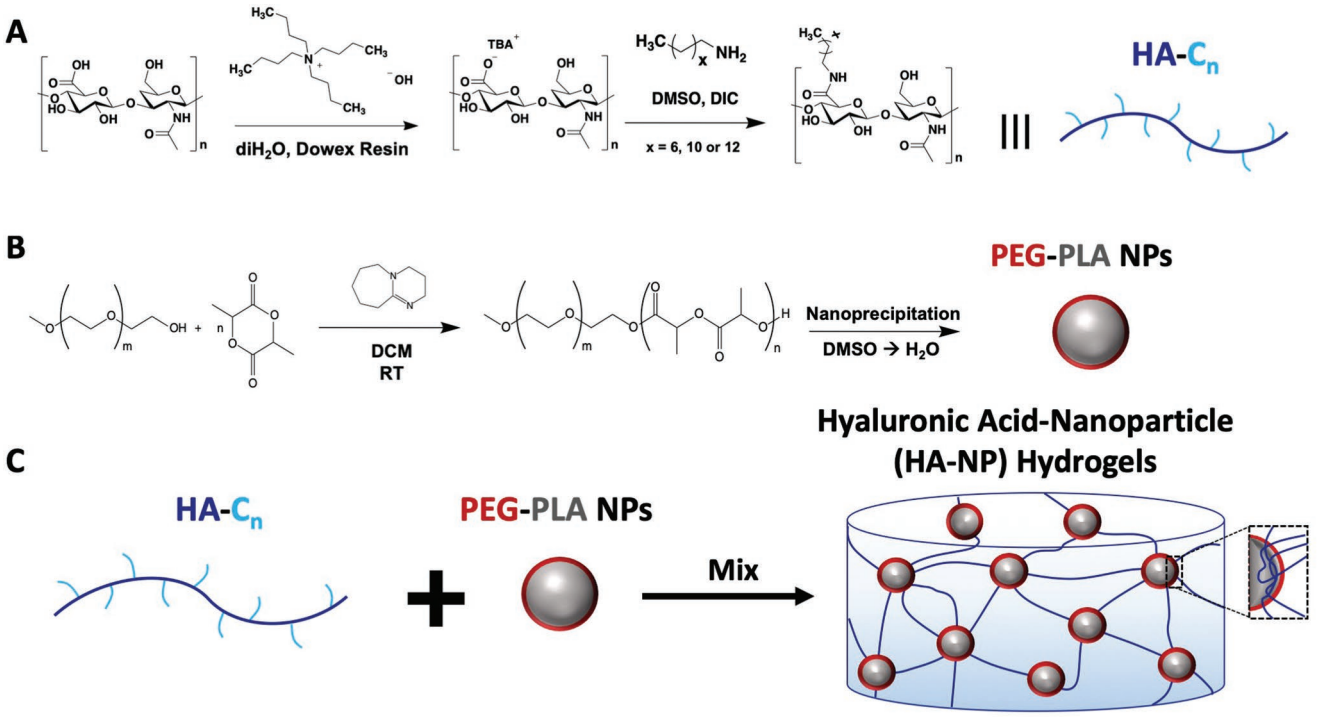


**Figure 1.** Fabrication of the HA–NP hydrogels from hyaluronic acid and biodegradable nanoparticles. A) Schematic representation of the chemical preparation of the hydrophobically-modified hyaluronic acid and B) core–shell poly(ethylene glycol)-block-poly(lactic acid) (PEG–PLA) nanoparticles (NPs). C) Upon mixing the HA–$C_n$ polymers (where $n$ = 8, 12, or 14) and the PEG–PLA NPs, a dynamic polymer–NP network is created.

functionalization or protein engineering.[16,17] Based on these approaches, we sought to synthesize a biocompatible, biomimetic hydrogel harnessing polymer–NP interactions between naturally occurring hyaluronic acid (HA) crosslinked by poly(ethylene glycol)-*block*-poly(lactic acid) (PEG-PLA) NPs. Hyaluronic acid is found ubiquitously throughout the body within extracellular matrix and is crucial for many cellular and tissue functions, including cellular communication, wound repair, morphogenesis, and matrix organization.[24] Further, HA has been approved by the Food and Drug Administration (FDA) for a number of clinical indications, and has demonstrated use in regenerative medicine due to its intrinsic biological signaling capabilities.[3,8,12,24–27]

In this contribution, we report the design of a new family of hyaluronic acid–nanoparticle (HA–NP) hydrogels with notable shear-thinning and self-healing behavior, derived from FDA-approved products (**Figure 1**). We hypothesized that development of HA–NP hydrogels would allow for improved injection mechanics, while maintaining the native regenerative properties of HA. We demonstrate that the HA–NP hydrogels form almost immediately upon mixing hydrophobically-modified HA with core–shell NPs. These hydrogels are governed by strong, yet reversible polymer–NP interactions, with the capacity to be delivered via a long, narrow catheter. Additionally, we demonstrate that hydrophobic chemical modification of the HA backbone does not interfere with its biochemical signaling capabilities. Finally, we highlight the differential therapeutic release mechanisms of HA–NP hydrogels and confirm in vivo biocompatibility following subcutaneous and intramuscular injection.

## 2. Results

### 2.1. Design and Synthesis of HA–NP Components

HA is a naturally occurring, linear polysaccharide found abundantly throughout extracellular matrix. We chose HA as the main polymer backbone due to its role in cellular survival, proliferation, and migration, as well as its particular relevance in tissue repair.[28] Furthermore, HA can be chemically modified through numerous means.[24] In this study, we modified HA with either tetradecylamine, dodecylamine or octylamine and achieved reproducible hydrophobic functionalization of 90–100%, determined by $^1$H NMR (Figure S1, Supporting Information). Additionally, we chose to synthesize PEG–PLA NPs due to their established in vivo biocompatibility and biodegradability in a variety of applications as drug delivery vehicles.[17,29] We created core–shell NPs in a reproducible and scalable manner via nanoprecipitation with a diameter size of ≈28 nm (Figure S2, Supporting Information).

### 2.2. HA–NP Hydrogel Formation and Mechanics

HA–NP hydrogels were formed by mixing aqueous solutions of the hydrophobically modified HA–$C_n$ polymers (where $n$ = 8, 12, or 14) and PEG–PLA NPs. The hydrogels formed rapidly upon mixing under ambient and physiologic conditions. Scanning electron micrograph (SEM) analysis demonstrated the general morphologic structure of the polymer chains (Figure S3, Supporting Information), exhibiting the homogenous distribution. Similarly,

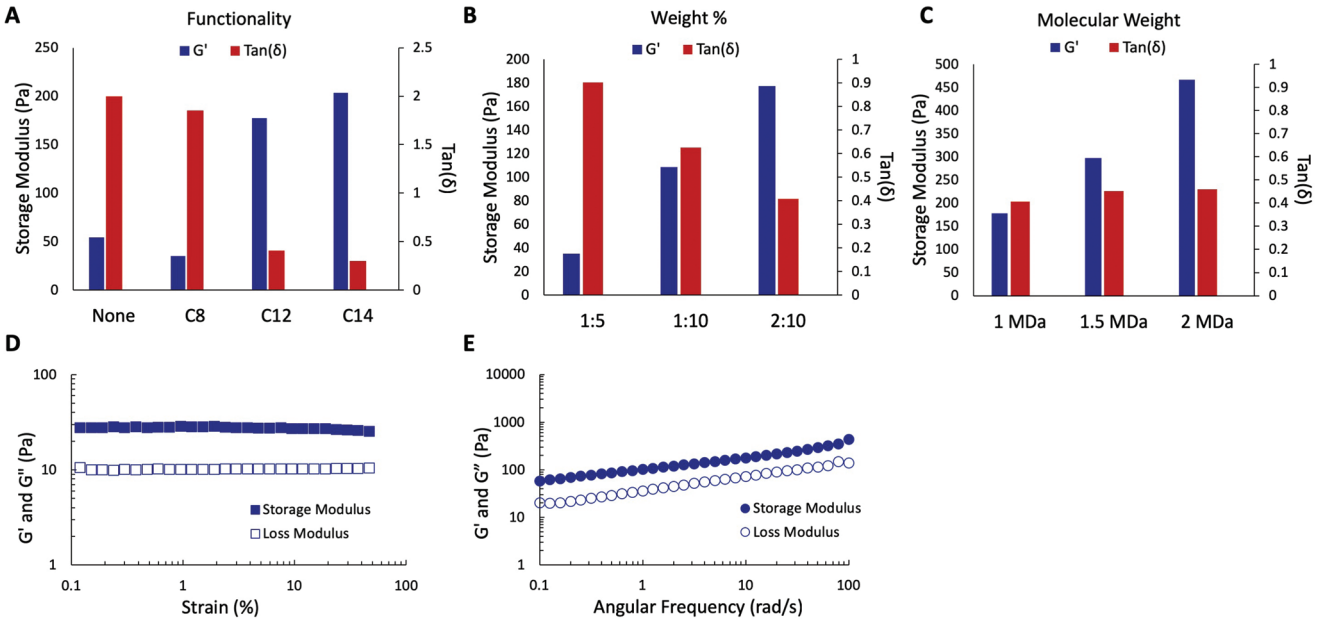


**Figure 2.** Rheological characterization of the HA–NP hydrogel family. Oscillatory rheology was performed to investigate A) HA–NP functionality with variable carbon chain lengths, B) HA–$C_{12}$ at various polymer loading (HA–$C_{12}$ wt%: NP wt%), and C) HA–$C_{12}$ with various molecular weights. D) Strain-dependent and E) frequency-dependent oscillatory shear rheology of 1 MDa HA–$C_{12}$ (2 wt%):NP (10 wt%) hydrogels.

cryogenic transmission electron microscopy highlighted the homogeneity of the NPs distributed throughout the hydrogel structure, indicating the network is formed via polymer–nanoparticle interactions.

For rheological characterization, we used the storage modulus ($G'$) as a measure of hydrogel strength measured at 10 rad $s^{-1}$. Tan $\delta$, the ratio of loss modulus ($G''$) over $G'$ (tan $\delta = G''/G'$), was used as a determination of the gelation point, where tan $\delta > 1$ denotes that the sample behaves more like a viscous fluid whereas tan $\delta < 1$ indicates the sample behaves as an elastic solid.[30] Oscillatory rheology revealed that mixing non-functionalized HA with PEG–PLA NPs created a viscous fluid (tan $\delta = 2.0$), indicating that hydrogel formation is exclusive to the presence of HA modified with highly hydrophobic chains. To determine the functionalization required for gelation, we formulated HA with octyl ($C_8$), dodecyl ($C_{12}$), or tetradecyl ($C_{14}$) functionality. HA–NP gels formed with HA–$C_8$ possessed similar properties to unmodified HA gels where fluid-like properties dominated (**Figure 2**A). However, HA–NP gels formed with HA–$C_{12}$ or HA–$C_{14}$ were roughly three to four times stronger, respectively, indicating interaction between the $C_{12}$ and $C_{14}$ moieties and the NPs to create a solid-like state. These observations are further supported by the fact that HA–$C_{12}$ polymers exhibit a dominant viscous fluid behavior when not in the presence of NPs (Figure S4, Supporting Information).

Next, we determined the impact of polymer loading on hydrogel mechanics by changing the weight percent of the aqueous polymer and NP solutions. In Figure 2B, we demonstrate that decreasing the total polymer and NP weight percent (1:5), weakens the hydrogel, yet maintains the dominant elastic properties. This is likely due to a decreased number of polymer–NP interactions. Conversely, increasing the total HA–$C_{12}$ weight percent (2:10) increases the strength of the hydrogel ≈65% compared to the 1:10 formulation. Similarly, changing the molecular weight (MW) of the HA backbone has a pronounced effect on hydrogel strength (Figure 2C). Increasing the MW of the HA–$C_{12}$ backbone to 1.5 MDa increased the hydrogel strength by 67% and increasing the MW to 2 MDa increased strength by 164%, compared to 1 MDa HA–$C_{12}$. These data support a broad range of hydrogel strengths (≈13-fold) that can be accomplished by varying the hydrogel parameters. Finally, we assessed strain-dependent rheology of the intermediate HA–NP gel (2 wt% HA–$C_{12}$: 10 wt% NPs, Figure 2D) and observed an extremely broad linear viscoelastic region. Further, the frequency dependence of the storage and loss moduli verified the solid-like behavior since $G'$ was dominant across the entire range of frequencies, spanning three decades (Figure 2E). All other formulations exhibited similar strain-dependent and frequency-dependent behavior with the exception of HA–$C_8$, which exhibited fluid-like behavior over all decades (Figures S5 and S6, Supporting Information).

### 2.3. HA–NP Shear-Thinning and Self-Healing Behavior

We sought to investigate the shear-thinning behavior of the intermediate polymer–nanoparticle network, HA–$C_{12}$:NP (2 wt%:10 wt%). Performing a shear-rate sweep revealed that the hydrogel has a steady and pronounced decrease in viscosity from low ($\dot{\gamma} \approx 0.1$ $s^{-1}$) to high ($\dot{\gamma} \approx 100$ $s^{-1}$) shear rates, highlighting its superior injectability (**Figure 3**A). A similar trend was measured in other formulations, further verifying the notable shear behavior (Figure S7, Supporting Information). We then performed step-shear measurements to evaluate the recovery of the hydrogel following rupture under high shear, which is critical during injection through high-gauge needles (Figure 3B). We observed the hydrogel's ability to break and

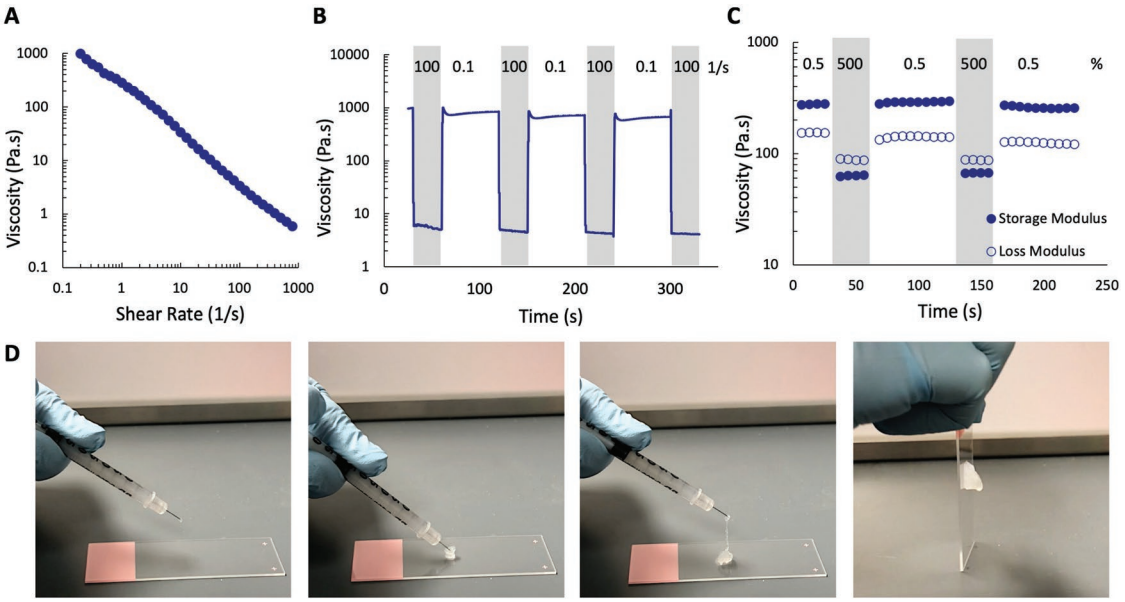


**Figure 3.** Shear-thinning and self-healing behavior of HA–NP hydrogels. A) Steady shear behavior of HA–$C_{12}$:NP (2 wt%:10 wt%) hydrogel over four decades of shear rate, demonstrating notable shear behavior. B) Step-shear measurements of HA–NP with high (100 $s^{-1}$) and low (0.1 $s^{-1}$) shear to demonstrate injectability and recovery. C) Step-strain measurements of HA–NP with high (500%) and low (0.5%) strains. D) Injectability of HA–NP hydrogel through a high gauge needle. The gel easily is injected through the syringe and rapidly re-heals to solid state demonstrated by the vertical slide.

reform over several cycles, which underlines the reversibility and strong polymer–NP crosslinks. Finally, we further delved into the extent of recovery of the hydrogel properties by performing repeated step-strain measurements. At high magnitude strains ($\varepsilon$ = 500%), the hydrogel structure was disrupted, and $G''$ was dominant, indicating fluid-like characteristics. However, at low magnitude strains ($\varepsilon$ = 0.5%), the hydrogel demonstrated rapid recovery of its solid-like characteristics. As a final assessment, we evaluated the injectability of the hydrogel by pushing it through a high-gauge (31-G) insulin syringe (Figure 3D). The hydrogel was easily injected through the syringe and immediately recovered its solid-like state upon exit from the needle and deposition on the slide. This is demonstrated by turning the slide vertically and the hydrogel remaining stationary. The rheology of the HA–NP hydrogels confirms the robust interaction between the HA—$C_{12}$ polymer and the PEG–PLA nanoparticles. This network is driven by the favorable energetics of the hydrophobic $C_{12}$ chain adsorption to the NPs. Additionally, the strong yet reversible polymer–NP crosslinks allows the hydrogel to be easily injected through a 31-G needle, demonstrating its superior capacity for minimally invasive delivery.

### 2.4. HA–NP Hydrogel Catheter Delivery

A critically unmet need in the field of hydrogels for cardiovascular tissue engineering is the ability to be delivered through a clinically relevant catheter. We sought to determine whether our hydrogel could be injected through a 4-Fr catheter affixed with a high-gauge needle. The correlation between injection force (i.e., pressure) and flow rate with properties of shear-thinning fluids has been described previously and indicates that our gels should be injectable by hand.[16,31,32] Indeed, we were able to easily inject the gel through the catheter. Immediately after injection, we performed rheological analysis to determine whether the hydrogel properties were changed by the catheter (**Figure 4**). Frequency sweep analysis revealed that the strength of the hydrogel was largely unchanged ($G' \approx$ 167 kPa post-catheter versus $G' \approx$ 177 kPa pre-catheter). This small change can be attributed to the priming of the catheter with phosphate buffered saline (PBS), which recapitulates the clinical scenario. Furthermore, the frequency sweep is nearly identical between the hydrogel both pre- and post-catheter injection, indicating that mechanics of the HA–NP hydrogel are unaffected by the catheter delivery.

### 2.5. HA–NP Hydrogel In Vitro Cytocompatibility

Hyaluronic acid has established proliferative, proangiogenic, and immunomodulatory effects.[33] Due to the addition of hydrophobic carbon chains, we sought to determine whether the HA component maintained its biocompatibility, cellular signaling properties, and regenerative effects. We first measured cellular viability in the presence or absence of the hydrogels. Fibroblasts were cultured in serum-free media and placed into hypoxia for 4 h in order to mimic stresses relevant in regenerative medicine applications such as ischemia. Following hypoxic incubation, we measured viability via an ATP-based viability assay. Luminescence analysis indicated that HA–NP significantly increased the viability of oxygen-starved fibroblasts by 1.9-fold compared to untreated media (**Figure 5**A). Additionally, we also observed the migratory effects of the HA–NP hydrogel utilizing a transwell migration assay. Endothelial progenitor cells significantly migrated towards the HA–NP hydrogel approximately 1.7-fold higher than PBS (Figure 5B). Finally, we evaluated the biocompatibility of the

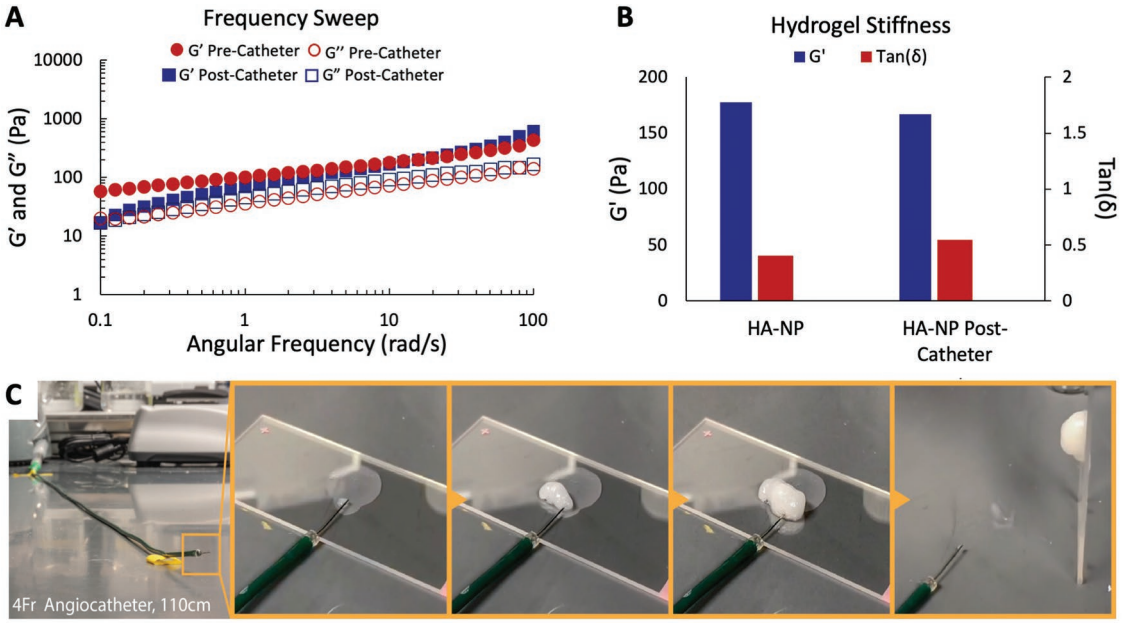


**Figure 4.** Hydrogel delivery through a clinically relevant injection catheter. A) Frequency-dependent oscillatory shear rheology of HA–NP hydrogel before and after catheter delivery. B) Hydrogel stiffness before and after catheter delivery. Oscillatory rheological properties of HA–NP are largely unchanged after catheter delivery. C) Image sequence of HA–NP delivery through a 110 cm, 4-Fr angiocatheter with a high gauge needle. Gel remains stationary following vertical movement of slide.

HA–NP hydrogel in an unstressed environment. The viability of human umbilical cord endothelial cells (HUVECs) cultured with hydrogel supernatant remained unchanged compared to HA only and untreated controls (Figure 5C,D). Across all experimental groups, cellular viabilities were ≈96%. These data support that the HA–NP hydrogel maintains the biocompatibility and therapeutic cell-signaling properties of HA.

### 2.6. HA–NP Differential Release and Therapeutic Efficacy

To determine the effect of the dual-loading potential of the HA–NP hydrogel, we measured the release of a 4 kDa fluorescently-conjugated therapeutic peptide from both phases of the gel for 7 d (**Figure 6**). This peptide was engineered in our laboratory as a more potent form of stromal cell derived factor-1$\alpha$ (SDF-1$\alpha$)

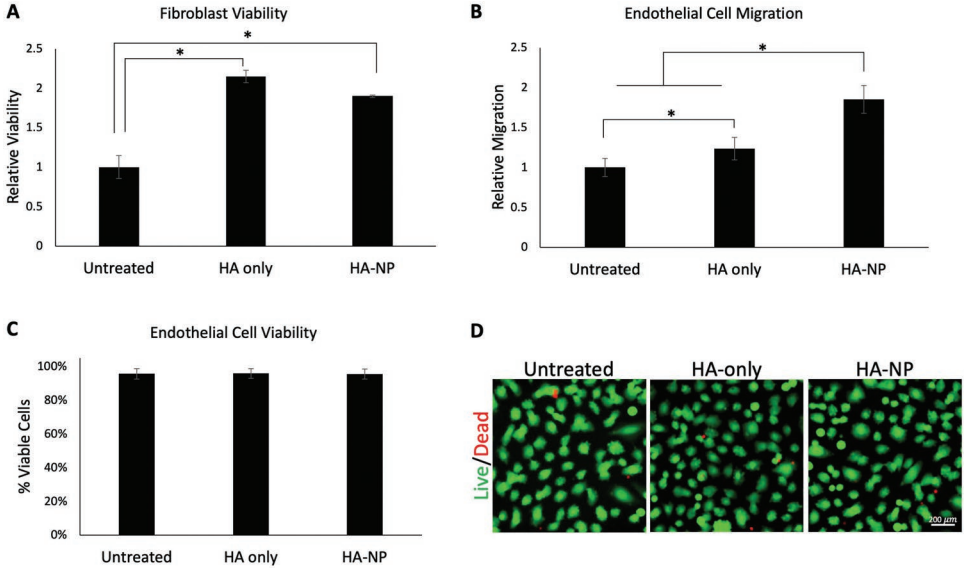


**Figure 5.** Cell signaling behavior of HA–NP hydrogels. A) Fibroblasts cultured under hypoxic conditions had a significant increase in cellular viability. B) Human umbilical cord vein endothelial cells (HUVECs) had significant migration toward the HA–NP hydrogel compared to the other treatment groups highlighting the ability of the HA–NP hydrogel to maintain its native HA signaling properties. C,D) Live/Dead cellular viability measurements of HUVECs in the presence of hydrogel. There were no differences in cellular morphology or viability between HA–NP and control groups (*$p < 0.05$).

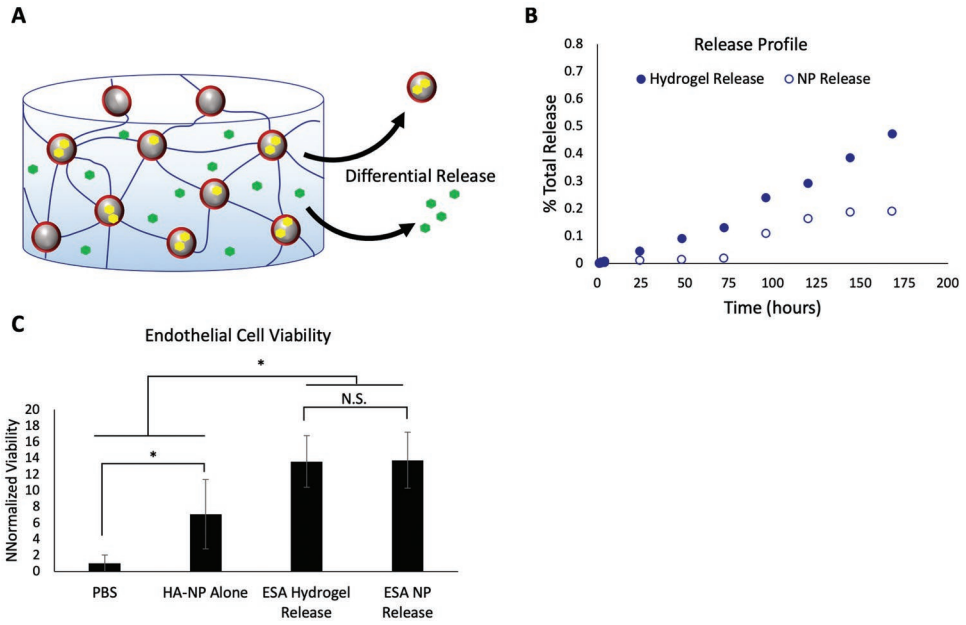


**Figure 6.** Differential release profiles. A) Schematic representation of the dual-release mechanism of the HA–NP hydrogels. Therapeutics can be encapsulated both in the nanoparticle phase and the aqueous phase within the hydrogel. B) Release profiles of an angiogenic peptide over a period of 7 d, demonstrating distinct elution profiles from the HA–NP hydrogel. C) Therapeutic activity of the encapsulated peptide. Engineered stromal cell derived factor 1$\alpha$ (ESA) released from both phases of the hydrogel (polymer phase and nanoparticle phase) resulted in a significant increase in cellular viability under hypoxic conditions ($^*p < 0.05$).

and is therefore a relevant angiogenic therapy that could potentially be released by this hydrogel in vivo. First, engineered SDF-1$\alpha$ (ESA) was loaded and released from the NP phase of the hydrogel. DLS analysis revealed that ESA loading did not affect the size of the NPs (Figure S3, Supporting Information). We observed a slow and steady release, with only 20% of the peptide being released after 7 d in solution. The ESA was also mixed into the aqueous phase of the hydrogel, and we observed a faster release, with ≈47% of the peptide being released from the gel after 7 d. Control over the release profile is advantageous for therapeutic timing. For example, SDF-1$\alpha$ expression and the expression of its receptor, CXCR4, are mismatched during myocardial ischemia; thus, controlled release would enhance therapeutic efficacy by normalizing the therapeutic window.[2,34]

To demonstrate that the bioactivity of the encapsulated peptide is retained following release from the hydrogel, we tested the proliferative capacity of ESA on HUVECs. As described, ESA is a truncated variant of SDF-1$\alpha$ that retains its therapeutic profile, and thus is capable of inducing proliferation in endothelial cells.[35–37] We evaluated ESA that eluted from the nanoparticle phase and the polymer phase of the hydrogel and compared to untreated controls. On HUVECs that were serum-starved and in hypoxia, ESA eluted from both phases of the hydrogel resulted in a 12-fold increase in cellular viability compared to the untreated PBS group (Figure 6C). These data support that the therapeutic effect is preserved when encapsulating the ESA into either phase of the hydrogel.

### 2.7. HA–NP In Vivo Biocompatibility

Finally, we aimed to determine the biocompatibility of the HA–NP hydrogel. Male Wistar rats were injected with 100 µL of the HA–NP hydrogel or 100 µL of PBS. Skin samples were explanted either on day 3 ($n = 3$ per group), day 7 ($n = 3$ per group), or day 14 ($n = 4$ per group) based on the degradation profile of the hydrogel (Figure S8, Supporting Information). A pathologist blinded to the treatment groups determined that there were no differences between the skin samples in the epidermis, dermis or subcutis (**Figure 7**). On day 3, there was mild infiltration of macrophages observed in the panniculus carnosus in rats treated with the hydrogel, likely due to phagocytosis of the material. However, there was not a significant number of neutrophils, lymphocytes, or other immune cells (Figure 7D). At days 7 and 14, inflammation had subsided and there was no presence of edema, granulation tissue, necrosis nor fibrosis (Figure 7E,F).

Additionally, we sought to investigate the biocompatibility of the HA–NP hydrogel in a second tissue type, namely, muscle. Wistar rats received 100 µL intramuscular (IM) injections of HA–NP hydrogel and muscles were harvested at day 3, day 7, and day 14. On day 3, we observed a mild infiltration of macrophages, consistent with a general inflammatory response localized to the injected site. By day 7 and day 14, the inflammatory response had completely subsided, with no evidence of edema, granulation tissue, necrosis nor fibrosis (Figure S9, Supporting Information).

### 2.8. HA–NP In Vivo Hemocompatibility

Due to the diverse applications of this hydrogel, it is important to evaluate the hemocompatibility of this material. In cardiovascular applications, it is critical to determine whether leakage of the material into the bloodstream is a potential

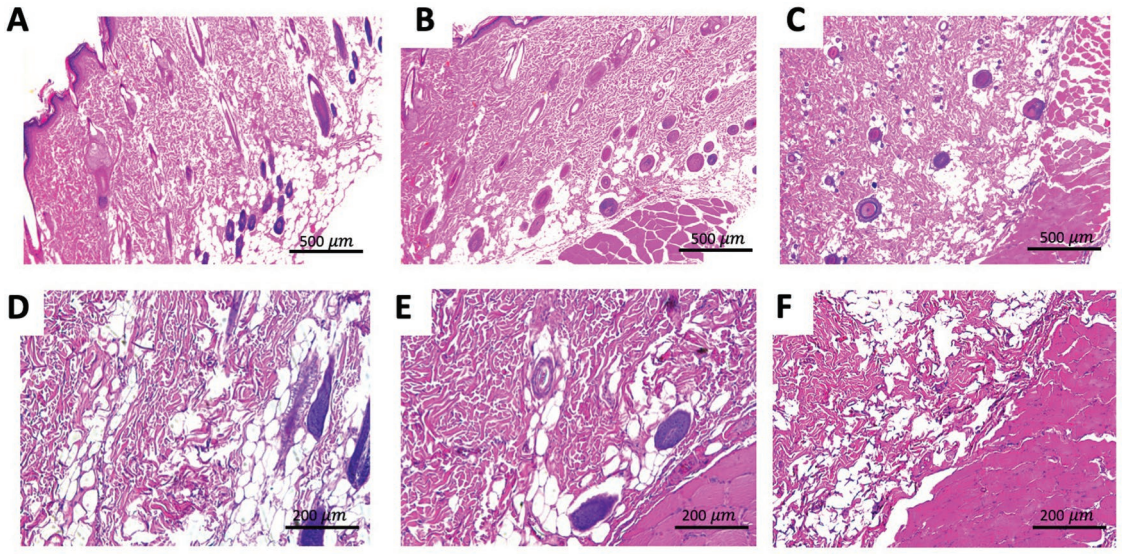


**Figure 7.** Representative H&E images of skin samples in contact with the HA–NP hydrogel. A) Day 3, B) day 7, and C) day 14 post subcutaneous injection. D) 10× Day 3, E) 10× Day 7, and F) 10× Day 14 H&E samples.

risk. Therefore, Wistar rats underwent intracardiac injections of either HA–NP or PBS to address the risk of embolization. Following injections, we observed no signs of stroke or gross morbidities. After 7 d, rats were sacrificed and underwent full necropsies. There was no difference between groups in any of the soft tissues (i.e., brain, heart, lung, kidneys) examined on histology.

## 3. Discussion

Over the last few decades, there has been a surge in the development of injectable biomaterials for tissue engineering and regenerative medicine applications.[4,38,39] Hydrogels are especially advantageous due to their high-water content, which mimics extracellular matrix elasticity and promotes biocompatibility. Injectable hydrogels can be used as vehicles to deliver cells, growth factors, and other small molecules, localizing these therapeutics to the intended area of treatment, effectively increasing their half-lives and serving as a sustained delivery reservoir for controlled release.[7,11,40] Additionally, acellular or a-therapeutic injectable hydrogels have demonstrated promise as tissue bulks or artificial tissue mimetics.[8,15,41]

Injectable hydrogels are desirable due to their ability to be delivered in a minimally invasive manner, which can occur via two major categories.[42] The first approach utilizes in situ gelation, in which the solid phase forms after the material has been injected. In this scenario, crosslinking occurs either during or after the injection, requiring a dual-barreled syringe or an external trigger.[43] This method presents numerous disadvantages because gelation is time-sensitive, thus risking material/cargo dispersion and loss following injection if gelation occurs too slowly.[44] Alternatively, if gelation occurs too quickly, the gel can clog the syringe and prevent delivery.[40,45] In situ gelation is therefore not realistic for catheter-based delivery techniques, which are crucial to advancing the field of hydrogels, particularly for cardiovascular tissue engineering, interventional radiology, and oncology.

The second approach exploits shear-thinning and self-healing behavior, viscoelastic properties which allow hydrogels to flow and re-heal into solid structures with the application and release of a shear force, respectively. Shear-thinning is defined as the ability of a viscoelastic material to have a decreasing viscosity with an increasing shear rate. During an applied shear force, as in the case of needle injection, the crosslinks within the hydrogel break, allowing the hydrogel to flow as a fluid. Upon removal of that shear force, the crosslinks reform and the hydrogel re-heals into a solid-like structure.[15,46,47] This approach allows for significant clinical translation due to enhanced injectability and a reduced chance of material and cargo loss.

Shear-thinning, self-healing hydrogels have been investigated for a number of biomedical applications including cell and drug delivery, tissue regeneration, and tissue bulking.[3,7,12,41,48–50] However, current shear-thinning hydrogels are limited due to complex, multistep chemical functionalization or advanced protein engineering techniques, which are expensive and poorly scalable. Furthermore, many shear-thinning hydrogels do not exhibit shear profiles that are amenable to facile catheter-based delivery, limiting their injectability to low gauge needles (i.e., large diameter) or syringes.[17] As a result, we sought to develop a biocompatible, highly shear-thinning hydrogel suitable for catheter-based, minimally invasive delivery. Furthermore, we hypothesized that creating this hydrogel based on a naturally occurring, major component of extracellular matrix would enable enhanced therapeutic efficacy.

In this report, we developed a new family of shear-thinning, catheter-injectable hydrogels based on polymer–NP interactions. These strong, yet reversible interactions allow the hydrophobically modified HA chains and NPs to self-assemble into a hydrogel. Furthermore, the process of synthesizing these components only requires two steps and can easily be scaled for

human applications. This is a major improvement over multistep functionalization or recombinant protein engineering techniques, which can take months to create clinically relevant volumes. We based this hydrogel off of a high-molecular weight HA backbone, due to the numerous therapeutic effects observed with native HA. HA is found ubiquitously throughout the human body and, along with collagen, is one of the most abundant polymers in extracellular matrix.[28,33] HA has been FDA approved for numerous clinical applications including ophthalmologic drug delivery, viscosupplementation in osteoarthritis and as a dermal filler.[33] Further, HA demonstrates wound healing and regenerative effects through cellular processes including survival, proliferation, migration, and differentiation.[8,15,28] Finally, high molecular weight (HMW) HA (≥1 MDa) exhibits anti-inflammatory effects, whereas low molecular weight HA is proinflammatory.[33] We combined the modified HMW HA polymer with PEG–PLA NPs, which are biocompatible and can be used for controlled drug delivery.[17,51] The result is a biomimetic, translational, therapeutic hydrogel for in situ tissue engineering.

We exploited the polymer–NP interactions to create a strong, versatile biomimetic hydrogel, which exhibits notable shear-thinning and self-healing behavior, that is capable of being injected through high-gauge needles and long, narrow, clinically relevant catheters. By varying the functionalization, polymer loading and MW of the HA backbone, we demonstrated >13-fold range in hydrogel strengths. Due to the potential of diverse applications with this family of hydrogels, we chose to further investigate the 2:10 HA−$C_{12}$:NP hydrogel, which demonstrated an intermediate stiffness within the wide range. Depending on the tissue of interest or release profile of interest, a variety of stiffnesses may be required. Thus, the intermediate hydrogel served as a representative, or average, of the behavior of the family. As a result, we demonstrated that the HA–NP hydrogel retains its cellular signaling properties via enhancing viability and stimulating chemotaxis during hypoxic conditions. Further, under standard physiologic conditions, cells retain a normal morphology and viability when cultured in the presence of the material.

We capitalized on the differential loading capabilities of this hydrogel for controlled drug release, demonstrating that we can deliver distinct release profiles of the same peptide. This can be advantageous for complex pathophysiology, which may require different signals at distinct times for optimal healing. In future studies, we will load different peptides into this gel to match the temporal and biological needs of various disease mechanisms. For example, this hydrogel could be used to address the temporal mismatch between the peak expression of SDF-1$\alpha$ and upregulation of its receptor, CXCR4 during ischemia for cardiac regeneration.[2] Importantly, we ensured that the peptide maintained its therapeutic effect following encapsulation into both phases of the hydrogel. The ESA peptide released from both the nanoparticle phase and the polymer phase significantly enhanced the viability of hypoxia-stressed endothelial cells, indicating that the therapeutic effect was retained.

Finally, we explored the in vivo translatability of this hydrogel by evaluating in vivo biocompatibility and hemocompatibility in a small animal model. We performed subcutaneous and intramuscular injections of the HA–NP hydrogels compared to a PBS control and subsequently harvested the tissue 3, 7, or 14 d postimplantation. Histological analysis revealed no significant difference in immunological response, with no significant infiltration of neutrophils or presence of fibrosis. In the event this material is used for cardiovascular applications, such as intramyocardial delivery, it is crucial to examine the hemocompatibility of this material in case the hydrogel leaks into the bloodstream. Rats that received an intracardiac injection of HA–NP had no observable gross or histological differences when compared to rats who received a PBS injection. However, it is important to consider the limitation of this experiment. It is possible that greater leakage of the material could occur in the clinical scenario of transendocardial delivery. Thus, our material demonstrated hemocompatibility at small volumes, but larger doses will need to be tested in the future to fully evaluate hemocompatibility for this particular application. Additionally, for this study we implemented a custom catheter design to test our hydrogel, which was created using an FDA-approved 4-Fr angiocatheter that was secured with a 28-G needle. There are currently other cardiac injection catheters that are under review for FDA approval, which exhibit smaller internal diameters compared to a 4-Fr catheter. Therefore, it is possible that a custom catheter would be necessary for use with this material. Nonetheless, our studies support the claim of catheter deliverability, which significantly enhances the clinical translation of this material.

## 4. Conclusion

Current injectable hydrogels are lacking appropriate mechanics and are limited by nonclinically translatable synthesis processes. In this work, we present a novel highly shear-thinning, self-healing hydrogel based on a naturally occurring polymer ubiquitous in the extracellular matrix. The transient and reversible hydrophobic interactions between the chemically-modified HA and the NPs allow this gel to be driven easily through a catheter, drastically enhancing its clinical promise by allowing minimally invasive delivery. Furthermore, this hydrogel retains its cellular signaling properties and demonstrates significant biocompatibility, with the ability to deliver drugs by differential mechanisms. Overall, we have overcome the main limitations of injectable hydrogels, and have developed a biomimetic, catheter-injectable hydrogel which can be used for controlled in vivo drug delivery.

## 5. Experimental Section

*Synthesis of HA–$C_n$ Polymers*: All chemicals were purchased from Sigma Aldrich unless otherwise noted. Hyaluronic acid was converted to its tetrabutylammonium salt (HA-TBA) via an established protocol.[52] Briefly, sodium hyaluronate (NaHA) (1, 1.5, and 2 MDa, Lifecore) was dissolved in deionized $H_2O$ (di$H_2O$) to give a 1 w/v% solution. Dowex 50W proton exchange resin (Acros Organics) was added to the solution (3 g of resin per 1 g of NaHA) and allowed to exchange for 6 h. The resin was removed, and the solution titrated to a pH of 9 with TBA-OH (Fisher Scientific O4575-100). The resulting solution was frozen at −80 °C, lyophilized, and stored at −20 °C for future use. To create

HA–$C_n$ (where $n$ = 8, 12, or 14), HA-TBA was dissolved in dimethyl sulfoxide to give a 0.5 w/v% solution. The resulting solution was heated to 45 °C, at which point, octylamine, dodecylamine, or tetradecylamine, and *N,N′*-diisopropylcarbodiimide were added in molar excess to the HA-TBA repeat unit. The reaction was allowed to proceed for 24 h, at which time, the solution was transferred to 3.5 kDa dialysis tubing, and dialyzed against $0.05 \times 10^{-3}$ M NaCl for 24 h. Finally, the solution was dialyzed against deionized water for an additional 72 h. The resulting solution was frozen at −80 °C, lyophilized, and stored long term at −20 °C.

*PEG–PLA Nanoparticle Synthesis*: Biodegradable PEG–PLA nanoparticles were created as previously described.[17] Briefly, 250 mg of PEG (5 kDa) and 10 µL of 1,8-diazabicyclo[5.4.0]undec-7-ene (DBU) were dissolved in dichloromethane (DCM; 1.0 mL). Lactide (1.0 g) was dissolved in 3 mL of DCM, and the resulting solution was added to PEG/DBU solution and stirred rapidly for 15 min. The reaction was quenched by adding the reaction solution to a solution of 15 mL of hexane and 15 mL of diethyl ether and subsequently vortexed. The hexane/ether solution was decanted, and the remaining PEG–PLA was dried overnight in a desiccator.

To create NPs, dried PEG–PLA (50 mg) was dissolved in DMSO (1 mL) and the solution was added dropwise to MilliQ water at a rapid stir rate. Resulting NPs were concentrated via filter ultracentrifugation (MWCO 10 kDa, Millipore Amicon Ultra-15) followed by resuspension in MilliQ water to a final concentration of 150 mg $mL^{-1}$. NP size and dispersity were characterized by dynamic light scattering (DLS).

*NMR Polymer Characterization*: $^1$H NMR spectra were recorded using a Varian Inova 300 MHz NMR spectrometer. Chemical shifts are recorded in p.p.m ($\delta$) in deuterium oxide with the internal reference peak set to $\delta$ = 4.80 p.p.m. Reaction products and polymer functionalization was assessed using MNOVA analysis software (Mestrelab Research).

*HA–NP Hydrogel Preparation*: Hydrogels were created by first dissolving HA–$C_n$ polymer in MilliQ water to give a 3 or 6 wt% solution. The 3 or 6 wt% solution and 15 wt% NP solution were added together to give a final solution of 1 wt% HA–$C_n$ or 2 wt% HA–$C_n$ polymer and 10 wt% NPs, respectively. The mixture was vortexed to ensure homogenous distribution, and then centrifuged to remove any bubbles. For each hydrogel formulation, the amount of HA–$C_n$ polymer solution and NP solution was varied and indicated by the given formulation name (HA–$C_n$ (wt%):NP (wt%)). All in vitro and in vivo experiments were conducted with 2:10 HA–$C_{12}$:NP due to its intermediate mechanical behavior.

*Polymer Characterization*: Rheological characterization was performed using a TA Instruments DHR-2 hybrid rheometer fitted with a Peltier stage. All measurements were conducted using the following parameters unless otherwise noted. Oscillatory frequency sweep measurements were conducted between 0.1 and 100 rad $s^{-1}$ with a torque of 2 µN m. Flow rate sweep measurements were conducted with shear rates between 0.1 and 1000 $s^{-1}$. Step-shear flow measurements were performed at shear rates of 0.1 and 100 $s^{-1}$. Step-strain oscillation measurements were conducted at 0.5% and 500% strain and an angular frequency of 10 rad $s^{-1}$. Oscillatory strain amplitude sweep measurements were carried out at a frequency of 10 rad $s^{-1}$ and torque was swept from 0.1 to 100 µN $m^{-1}$. All tests were performed using a 20 mm plate geometry and a Peltier temperature of 37 °C with a gap height of 1000 µm. Analysis was performed using TA Instruments TRIOS software.

*Morphological Characterization*: Cryogenic TEM (CryoTEM) images were acquired using a FEI Tecnai G2 F20 X-TWIN transmission electron microscope equipped with a Gatan K2 summit direct detection device. Prior to imaging 3 µL of the hydrogel sample was transferred to a 200 mesh Lacey carbon copper grid (Electron Microscopy Sciences). A Leica EM GP was used to remove excess fluid and plunge freeze the samples in liquid ethane. Samples were immediately transferred to the CryoTEM for imaging.

SEM images were acquired with an FEI Magellan 400 XHR Microscope with a beam voltage of 1.5 V. Lyophilized hydrogel samples were pressed onto carbon paint and sputter-coated with Au:Pd (60:40) before imaging.

*Hydrogel Erosion Assay*: A uronic-acid based, colorimetric assay was used to determine the in vitro erosion profile of the HA–NP hydrogel based on an established protocol.[53,54] Briefly, 100 µL of hydrogel was added to a 1.5 mL Eppendorf tube and quickly centrifuged to remove any entrapped air. Subsequently 1 mL of PBS was then added to the tube ($n$ = 4). At 3, 7, 10, and 14 d, the PBS was carefully removed and collected before being replaced with 1 mL of fresh PBS. On day 14, the remaining gel was disrupted using 1 mg $mL^{-1}$ hyaluronidase from bovine testes (Sigma-Aldrich, 3506). The uronic acid concentration was measured using a carbazole reaction as described previously.[53] 50 µL of each sample was added to a glass vial followed by 1 mL of ice-cold $25 \times 10^{-3}$ M sodium tetraborate in concentrated sulfuric acid. Vials were incubated for 10 min at 100 °C and then were cooled on ice at which point, 30 µL of 0.125% (wt/vol) carbazol (Sigma-Aldrich, C5132) in absolute ethanol was added before briefly vortexing. Vials were then incubated for 15 min at 100 °C. Following incubation, the vials were allowed to cool to room temperature and 200 µL of the solution was transferred to a 96-well plate for measurement. The absorbance at 525 nm was read using a plate reader (Synergy 2 BioTek Microplate reader, BioTek Instruments).

*Catheter Development and Test*: To create the injection catheter, a 28-G needle was incorporated into a 4Fr angiocatheter. The needle was fitted to the diameter (≈1.0 mm) of the catheter and secured via epoxy glue. The epoxy was allowed to dry overnight. Prior to the injection test, the catheter was primed with ≈200 µL of PBS to mimic in vivo application. Next, 3 mL of HA–NP was loaded into a syringe and pressure was applied. After the PBS visibly exited the catheter, we began collecting the HA–NP gel. Immediately after ≈100 µL of hydrogel was injected through the catheter, we began rheology measurements. Rheological tests were performed as described above.

*In Vitro Fibroblast Viability Assay*: To assess the cytocompatibility of the HA–NP, NIH3T3 cells (ATCC CRL-1658) were plated in a 24-well plate (CELLTREAT) at a density of 50 000 cells per well. Two days prior to cell treatment, 100 µL HA–NP gels ($n$ = 8) or 100 µL of 2 wt% HA ($n$ = 7) were deposited into 0.4 µm pore transwells (CorningTranswell) and allowed to elute into serum-free DMEM. When the cells reached confluency, 300 µL of eluent from each treatment group was added: serum-free DMEM ($n$ = 8), 2 wt% HA in serum-free DMEM, HA–NP gel in serum-free DMEM. The cells were stressed by incubation under hypoxic conditions for 4 hours at 1% oxygen, 5% carbon dioxide, 60% humidity and 37 °C (X3 Hypoxia Hood and Culture Combo from Xvivo System). Following incubation, cell viability reagent (Promega, G7570) was added to each well in an amount equal to the media. The plate was gently agitated and allowed to sit for 10 min at room temperature. Contents of the 24-well plate were transferred to a white 96-well plate and read on a luminescent plate reader (Synergy 2 BioTek Microplate reader, BioTek Instruments).

*Endothelial Cell Chemotaxis Assay*: A transwell chemotaxis assay (CytoSelect 96-Well Cell Migration Assay) was used to quantify HUVEC migration. Two days prior to the start of the assay, 100 µL HA–NP gel samples ($n$ = 6), 100 µL of 2 wt% HA ($n$ = 6), or 100 µL PBS ($n$ = 6) were prepared and deposited into 0.4 µm transwells and placed into 1 mL of PBS in a 24-well plate. On the day of the chemotaxis assay, HUVECs (Gibco LSC0035C) were thawed and counted. The bottom feeder tray was used to load the treatments: PBS only, PBS incubated with HA, or PBS incubated with HA–NP hydrogel. Cells were centrifuged and resuspended in PBS to be loaded into the top membrane chamber. The 96-well 8-µm membrane chamber was placed on top of the feeder tray and the HUVEC cell suspension loaded into each well at a density of 600 000 cells $mL^{-1}$. The plate was placed in a hypoxic incubator for 4 h (X3 Hypoxia Hood and Culture Combo from Xvivo System) at 1% oxygen, 5% carbon dioxide, 60% humidity and 37 °C. Upon removal of the plate from the incubator, cells were suctioned from the membrane chamber. The membrane chamber was then moved to the harvesting tray containing Cell Detachment Solution and incubated for 30 minutes. After incubation the membrane chamber was removed, and Lysis Buffer was added to each well in the harvesting tray and incubated again for 20 min. After incubation, the harvesting tray solution was removed and

added to a black 96-well clear-bottom plate. Fluorescence was read on a fluorescent plate reader at 485 nm/535 nm (excitation/emission) (Synergy 2 BioTek).

*Endothelial Cell Viability Assay*: To determine hydrogel biocompatibility, a Live/Dead assay kit was used to quantify the number of viable HUVECs in the presence of the hydrogel. HUVECs were plated at a density of 30 000 cells per well in a 96-well plated coated with Matrigel (Corning). Hydrogels were formed in 50 µL aliquots in Eppendorf tubes and subsequently submerged in 1.5 mL of endothelial cell growth media, EGM2 (Lonza). The hydrogels incubated in the media for 24 h, at which point the media was removed, and transferred to the HUVEC plate. The HUVECs were incubated with the treatment at physiologic conditions for 24 h. After 1 d, the Live Dead Assay Kit (Abcam, ab115347) was performed according to the manufacturer's protocol. The cells were then imaged on a fluorescent microscope (Leica DMi8) with a 10× objective and GFP/RFP filters.

*In Vitro Release and Bioactivity*: To measure the dual release mechanisms of the HA–NP hydrogel, a Cyanine7 (Cy7) fluorescently-tagged peptide was utilized. Our lab previously developed an engineered version of stromal cell-derived factor 1$\alpha$ (SDF-1$\alpha$), termed engineered SDF-1$\alpha$ (ESA), which has demonstrated potent angiogenic properties.[2,55,34,35] This peptide was used as a model therapeutic to be released from the hydrogel due to its use in regenerative medicine therapeutics such as an adjunct treatment for myocardial infarction.[2,56,57] ESA was synthesized using solid-phase peptide synthesis and a Cy7 fluorescent molecule was added (AnaSpec, San Jose, CA) during the synthesis process as a fluorescent marker during release.

To measure release from the nanoparticles, 100 µg of ESA-Cy7 NPs was prepared by co-nanoprecipitation of ESA-Cy7 with PEG–PLA block copolymer. The fluorescent signal was measured following NP ultracentrifugation to ensure that all ESA-Cy7 was contained within the NPs. These NPs were then used to prepare the hydrogels according to the protocol above. In the second experiment, 100 µg ESA-Cy7 was dissolved with the HA–$C_{12}$ polymer and then hydrogels were created as above to determine release from the aqueous phase. Hydrogels of either type were created ($n$ = 4, 100 µL each) and placed in 0.4 µm transwells, submerged in 1 mL of PBS in a 24 well plate (Corning) and release was measured daily for a period of 7 d. At each time point, the transwells were moved to a fresh well of 1 mL PBS. The collected aqueous solutions were analyzed for peptide concentration based on calibration curves prepared using ESA-Cy7 fluorescence (750 nm/773 nm excitation/emission).

To determine the activity of the ESA peptide after release, its therapeutic effect was examined on HUVECs due to SDF's proven proliferative effect on endothelial cells.[36] As described above, 100 µL of hydrogel was formed either with ESA–NPs (ESA NP release) or ESA dissolved into the HA–$C_{12}$ polymer phase (ESA Hydrogel release). Hydrogels of both types ($n$ = 4/group) were placed into transwells and submerged in 1 mL of PBS in a 24-well plate. Control wells containing PBS and HA–NP hydrogel alone ($n$ = 4 per group) were also created at this time. We allowed the peptide to elute from the hydrogels for 48 h. At this point, the eluted treatments (PBS, HA–NP alone, ESA hydrogel, and ESA–NP) were removed from beneath the transwells and placed onto HUVECs plated at 30 000 cells $mL^{-1}$ in a 96-well plate. The HUVECs were then transferred to hypoxia for 4 h at 1% oxygen, 5% carbon dioxide, 60% humidity and 37 °C. Following incubation, cell viability reagent (Promega, G7570) was added to each well in an amount equal to the media. The plate was gently agitated and allowed to sit for 10 min at room temperature. Contents of the plate were transferred to a white 96-well plate and read on a luminescent plate reader.

*In Vivo Biocompatibility*: All animal procedures were performed according to Stanford Animal Care and Use Committee approved protocols. For biocompatibility studies, male Wistar rats weighing ≈350 g were mildly sedated using inhaled 2% isoflurane and a section of fur shaved on their back. Rats were then injected subcutaneously in the back with HA–NP gels (100 µL, $n$ = 3 per time point) or with PBS (100 µL, $n$ = 3 per time point) using a 28-G insulin syringe. Injection site was marked via permanent marker. Likewise, for intramuscular tissue analysis, rats were injected with either 100 µL of HA–NP ($n$ = 4 per time point) or 100 µL of PBS ($n$ = 4 per time point) into the quadricep muscle. At days 3, 7, and 14 d following administration, rats were sacrificed, and the tissue surrounding the injection site (either skin or muscle) was harvested. Tissue was fixed in paraformaldehyde, and cross-sections of skin and muscle were embedded in paraffin and stained with haematoxylin and eosin (H&E). H&E and Masson's Trichrome analyses were performed by a pathologist who was blinded to the treatment groups.

*In Vivo Hemocompatibility*: To test hemocompatibility, Wistar rats weighing ≈250–300 g were sedated, intubated, and underwent a left thoracotomy. Due to our lab's extensive experience with small and large animal IM cardiac injections,[2,7,58,59] a maximum of 1–5% material leakage into the bloodstream was approximated. A typical IM cardiac injection in a rat is ≈100 µL. Therefore, the rats then received a 5 µL injection of HA–NP ($n$ = 3) or PBS ($n$ = 2) directly into the lumen of the left ventricle (intracardiac). One week following the intracardiac injections, rats were sacrificed, and full necropsies and histology were performed by a blinded pathologist.

*Statistical Analysis*: All analyzed in vitro data approximated a normal distribution and are reported as mean±standard deviation. Pairwise Student $t$ tests were used to evaluate statistical difference between variables with a Bonferroni correction used for multiple comparisons. For all statistical tests, a threshold value of $P < 0.05$ indicated significance.

## Supporting Information

Supporting Information is available from the Wiley Online Library or from the author.

## Acknowledgements

E.A.A. and Y.J.W. contributed equally to this work. A.N.S., L.M.S., Y.J.W., and E.A.A. designed experiments; A.N.S., J.M.F., H.J.L., M.J.P., A.E., C.H., A.T., H.W., A.C.Y., D.C. conducted experiments; A.N.S, L.M.S., Y.J.W., and E.A.A. analyzed data; and A.N.S., Y.J.W., and E.A.A. wrote paper. This study was supported in part by the National Institute of Health [NIH R01 HL089315-01 (Y.J.W.)] and Stanford BioX Interdisciplinary Initiatives Program Seed Grant (E.A.A.).

## Conflict of Interest

The authors declare no conflict of interest.

## Keywords

catheter delivery, drug delivery, hydrogels, nanoparticles, shear thinning

Received: September 13, 2018
Revised: January 10, 2019
Published online: February 4, 2019

[1] A. Hasan, A. Khattab, M. A. Islam, K. A. Hweij, J. Zeitouny, R. Waters, M. Sayegh, M. M. Hossain, A. Paul, *Adv. Sci.* **2015**, *2*, 1500122.
[2] J. W. MacArthur, B. P. Purcell, Y. Shudo, J. E. Cohen, A. Fairman, A. Trubelja, J. Patel, P. Hsiao, E. Yang, K. Lloyd, W. Hiesinger, P. Atluri, J. A. Burdick, Y. J. Woo, *Circulation* **2013**, *128*, S79.
[3] C. B. Rodell, J. W. MacArthur, S. M. Dorsey, R. J. Wade, L. L. Wang, Y. J. Woo, J. A. Burdick, *Adv. Funct. Mater.* **2015**, *25*, 636.

[4] X. Guan, M. Avci-Adali, E. Alarçin, H. Cheng, S. S. Kashaf, Y. Li, A. Chawla, H. L. Jang, A. Khademhosseini, *Biotechnol. J.* **2017**, *12*, 1600394.
[5] L. Saludas, S. Pascual-Gil, F. Prósper, E. Garbayo, M. Blanco-Prieto, *Int. J. Pharm.* **2017**, *523*, 454.
[6] J. E. Cohen, B. P. Purcell, J. W. MacArthur, A. Mu, Y. Shudo, J. B. Patel, C. M. Brusalis, A. Trubelja, A. S. Fairman, B. B. Edwards, M. S. Davis, G. Hung, W. Hiesinger, P. Atluri, K. B. Margulies, J. A. Burdick, Y. J. Woo, *Circ.: Heart Failure* **2014**, *7*, 619.
[7] A. N. Steele, L. Cai, V. N. Truong, B. B. Edwards, A. B. Goldstone, A. Eskandari, A. C. Mitchell, L. M. Marquardt, A. A. Foster, J. R. Cochran, S. C. Heilshorn, Y. J. Woo, *Biotechnol. Bioeng.* **2017**, *114*, 2379.
[8] E. Tous, J. L. Ifkovits, K. J. Koomalsingh, T. Shuto, T. Soeda, N. Kondo, J. H. Gorman, R. C. Gorman, J. A. Burdick, *Biomacromolecules* **2011**, *12*, 4127.
[9] B. A. Aguado, W. Mulyasasmita, J. Su, K. J. Lampe, S. C. Heilshorn, *Tissue Eng., Part A* **2012**, *18*, 806.
[10] G. Camci-Unal, N. Annabi, M. R. Dokmeci, R. Liao, A. Khademhosseini, *NPG Asia Mater.* **2014**, *6*, e99.
[11] A. N. Steele, J. W. MacArthur, Y. J. Woo, *Circ. Res.* **2017**, *120*, 1868.
[12] H. Wang, D. Zhu, A. Paul, L. Cai, A. Enejder, F. Yang, S. C. Heilshorn, *Adv. Funct. Mater.* **2017**, *27*, 1605609.
[13] H. Tan, K. G. Marra, *Materials* **2010**, *3*, 1746.
[14] J. L. Drury, D. J. Mooney, *Biomaterials* **2003**, *24*, 4337.
[15] C. B. Rodell, M. E. Lee, H. Wang, S. Takebayashi, T. Takayama, T. Kawamura, J. S. Arkles, N. N. Dusaj, S. M. Dorsey, W. R. T. Witschey, J. J. Pilla, J. H. Gorman, J. F. Wenk, J. A. Burdick, R. C. Gorman, *Circ.: Cardiovasc. Interventions* **2016**, *9*, e004058.
[16] J. L. Mann, A. C. Yu, G. Agmon, E. A. Appel, *Biomater. Sci.* **2017**, *6*, 10.
[17] E. A. Appel, M. W. Tibbitt, M. J. Webber, B. A. Mattix, O. Veiseh, R. Langer, *Nat. Commun.* **2015**, *6*, 6295.
[18] L. L. Wang, J. N. Sloand, A. C. Gaffey, C. M. Venkataraman, Z. Wang, A. Trubelja, D. A. Hammer, P. Atluri, J. A. Burdick, *Biomacromolecules* **2017**, *18*, 77.
[19] C. B. Rodell, C. B. Highley, M. H. Chen, N. N. Dusaj, C. Wang, L. Han, J. A. Burdick, *Soft Matter* **2016**, *12*, 7839.
[20] H. D. Lu, M. B. Charati, I. L. Kim, J. A. Burdick, *Biomaterials* **2012**, *33*, 2145.
[21] C.-C. Huang, S. Ravindran, Z. Yin, A. George, *Biomaterials* **2014**, *35*, 5316.
[22] W. Mulyasasmita, J. S. Lee, S. C. Heilshorn, *Biomacromolecules* **2011**, *12*, 3406.
[23] W. Mulyasasmita, L. Cai, R. E. Dewi, A. Jha, S. D. Ullmann, R. H. Luong, N. F. Huang, S. C. Heilshorn, *J. Controlled Release* **2014**, *191*, 71.
[24] J. A. Burdick, G. D. Prestwich, *Adv. Mater.* **2011**, *23*, H41.
[25] A. Fakhari, C. Berkland, *Acta Biomater.* **2013**, *9*, 7081.
[26] F. S. Brandt, A. Cazzaniga, *Clin. Interventions Aging* **2008**, *3*, 153.
[27] L. E. Miller, J. E. Block, *Clin. Med. Insights: Arthritis Musculoskeletal Disord.* **2013**, *6*, CMAMD.S12743.
[28] F. Bonafè, M. Govoni, E. Giordano, C. M. Caldarera, C. Guarnieri, C. Muscari, *J. Biomed. Sci.* **2014**, *21*, 100.
[29] N. Kamaly, Z. Xiao, P. M. Valencia, A. F. Radovic-Moreno, O. C. Farokhzad, *Chem. Soc. Rev.* **2012**, *41*, 2971.
[30] C. Yan, D. J. Pochan, *Chem. Soc. Rev.* **2010**, *39*, 3528.
[31] R. A. Chilton, R. Stainsby, *J. Hydraul. Eng.* **1998**, *124*, 522.
[32] S. N. López-Carranza, M. Jenny, C. Nouar, *C. R. Méc.* **2012**, *340*, 602.
[33] J. E. Rayahin, J. S. Buhrman, Y. Zhang, T. J. Koh, R. A. Gemeinhart, *ACS Biomater. Sci. Eng.* **2015**, *1*, 481.
[34] J. W. Macarthur, J. E. Cohen, J. R. McGarvey, Y. Shudo, J. B. Patel, A. Trubelja, A. S. Fairman, B. B. Edwards, G. Hung, W. Hiesinger, A. B. Goldstone, P. Atluri, R. L. Wilensky, J. J. Pilla, J. H. Gorman, R. C. Gorman, Y. J. Woo, *Circ. Res.* **2014**, *114*, 650.
[35] W. Hiesinger, J. M. Perez-Aguilar, P. Atluri, N. A. Marotta, J. R. Frederick, J. R. Fitzpatrick, R. C. McCormick, J. R. Muenzer, E. C. Yang, R. D. Levit, L.-J. Yuan, J. W. Macarthur, J. G. Saven, Y. J. Woo, *Circulation* **2011**, *124*, S18.
[36] C. R. W. Kuhlmann, C. A. Schaefer, L. Reinhold, H. Tillmanns, A. Erdogan, *Biochem. Biophys. Res. Commun.* **2005**, *335*, 1107.
[37] B. B. Edwards, A. S. Fairman, J. E. Cohen, J. W. MacArthur, A. B. Goldstone, J. B. Woo, W. Hiesinger, Y. J. Woo, *J. Vasc. Surg.* **2016**, *64*, 1093.
[38] K. L. Christman, R. J. Lee, *J. Am. Coll. Cardiol.* **2006**, *48*, 907.
[39] A. A. Rane, K. L. Christman, *J. Am. Coll. Cardiol.* **2011**, *58*, 2615.
[40] M. H. Chen, L. L. Wang, J. J. Chung, Y.-H. Kim, P. Atluri, J. A. Burdick, *ACS Biomater. Sci. Eng.* **2017**, *3*, 3146.
[41] J. L. Ifkovits, E. Tous, M. Minakawa, M. Morita, J. D. Robb, K. J. Koomalsingh, J. H. Gorman, R. C. Gorman, J. A. Burdick, *Proc. Natl. Acad. Sci. USA* **2010**, *107*, 11507.
[42] M. Guvendiren, H. D. Lu, J. A. Burdick, *Soft Matter* **2012**, *8*, 260.
[43] J.-A. Yang, J. Yeom, B. W. Hwang, A. S. Hoffman, S. K. Hahn, *Prog. Polym. Sci.* **2014**, *39*, 1973.
[44] A. T. Hillel, S. Unterman, Z. Nahas, B. Reid, J. M. Coburn, J. Axelman, J. J. Chae, Q. Guo, R. Trow, A. Thomas, Z. Hou, S. Lichtsteiner, D. Sutton, C. Matheson, P. Walker, N. David, S. Mori, J. M. Taube, J. H. Elisseeff, *Sci. Transl. Med.* **2011**, *3*, 93ra67.
[45] T. P. Martens, A. F. G. Godier, J. J. Parks, L. Q. Wan, M. S. Koeckert, G. M. Eng, B. I. Hudson, W. Sherman, G. Vunjak-Novakovic, *Cell Transplant.* **2009**, *18*, 297.
[46] G. N. Grover, R. L. Braden, K. L. Christman, *Adv. Mater.* **2013**, *25*, 2937.
[47] L. Yu, J. Ding, *Chem. Soc. Rev.* **2008**, *37*, 1473.
[48] L. Cai, R. E. Dewi, A. B. Goldstone, J. E. Cohen, A. N. Steele, Y. J. Woo, S. C. Heilshorn, *Adv. Healthcare Mater.* **2016**, *5*, 2758.
[49] M. J. Hernandez, K. L. Christman, *JACC: Basic Transl. Sci.* **2017**, *2*, 212.
[50] J. M. Singelyn, P. Sundaramurthy, T. D. Johnson, P. J. Schup-Magoffin, D. P. Hu, D. M. Faulk, J. Wang, K. M. Mayle, K. Bartels, M. Salvatore, A. M. Kinsey, A. N. Demaria, N. Dib, K. L. Christman, *J. Am. Coll. Cardiol.* **2012**, *59*, 751.
[51] R. Z. Xiao, Z. W. Zeng, G. L. Zhou, J. J. Wang, F. Z. Li, A. M. Wang, *Int. J. Nanomed.* **2010**, *5*, 1057.
[52] W. M. Gramlich, I. L. Kim, J. A. Burdick, *Biomaterials* **2013**, *34*, 9803.
[53] C. Loebel, C. B. Rodell, M. H. Chen, J. A. Burdick, *Nat. Protoc.* **2017**, *12*, 1521.
[54] J. A. Burdick, C. Chung, X. Jia, M. A. Randolph, R. Langer, *Biomacromolecules* **2005**, *6*, 386.
[55] W. Hiesinger, A. B. Goldstone, Y. J. Woo, *Trends Cardiovasc. Med.* **2012**, *22*, 139.
[56] A. B. Goldstone, C. E. Burnett, J. E. Cohen, M. J. Paulsen, A. Eskandari, B. E. Edwards, A. B. Ingason, A. N. Steele, J. B. Patel, J. W. MacArthur, J. A. Shizuru, Y. J. Woo, *J. Cardiovasc. Transl. Res.* **2018**, *11*, 274.
[57] T. K. Ho, X. Shiwen, D. Abraham, J. Tsui, D. Baker, *Cardiol. Res. Pract.* **2012**, *2012*, 1.
[58] J. E. Cohen, A. B. Goldstone, M. J. Paulsen, Y. Shudo, A. N. Steele, B. B. Edwards, J. B. Patel, J. W. MacArthur, M. S. Hopkins, C. E. Burnett, K. J. Jaatinen, A. D. Thakore, J. M. Farry, V. N. Truong, A. T. Bourdillon, L. M. Stapleton, A. Eskandari, A. S. Fairman, W. Hiesinger, T. V. Esipova, W. L. Patrick, K. Ji, J. A. Shizuru, Y. J. Woo, *Sci. Adv.* **2017**, *3*, e1603078.
[59] J. W. MacArthur, A. N. Steele, A. B. Goldstone, J. E. Cohen, W. Hiesinger, Y. J. Woo, *Curr. Treat. Options Cardiovasc. Med.* **2017**, *19*, 30.